Estuarine, Coastal and Shelf Science xxx (xxxx) xxx

Contents lists available at ScienceDirect

Estuarine, Coastal and Shelf Science

journal homepage: http://www.elsevier.com/locate/ecss

Mangrove leaf species-specific isotopic signatures along a salinity and phosphorus soil fertility gradients in a subtropical estuary

Ding He [a,b], Victor H. Rivera-Monroy [c,*], Rudolf Jaffé [b], Xiaochen Zhao [c]

[a] Institute of Geology, School of Earth Sciences, Zhejiang University, Hangzhou, Zhejiang, 310027, China
[b] Southeast Environmental Research Center and Department of Chemistry & Biochemistry, Florida International University, Miami, FL, 33199, USA
[c] Department of Oceanography and Coastal Sciences, College of the Coast and Environment, Louisiana State University, Baton Rouge, LA, 70803, USA

ARTICLE INFO

Keywords:
Mangroves
Carbon isotopes
Nitrogen isotopes
n-alkanes
Compound-specific carbon isotopes
Florida

ABSTRACT

Mangrove ecotypes are distinct monospecific or mix-species assemblages and used as classification criteria to evaluate coastal biogeochemical cycles at the local, regional, and global scales. However, it is not clear how plant nitrogen and carbon content, including bulk $\delta^{13}C$ and $\delta^{15}N$ and *n*-alkane $\delta^{13}C$ values, vary across species and within species when plants are exposed to the interaction between nutrient (nitrogen-N, phosphorus-P) availability and stressors (i.e., salinity). Here we present significant differences in green leaves wax *n*-alkane $\delta^{13}C$ ($\delta^{13}C_{n\text{-alkane}}$) values and brown-senescent leaves C:N atomic ratios and total phosphorus (TP) concentrations of three mangrove species (*Rhizophora mangle*, *Laguncularia racemosa*, and *Avicennia germinans*) that reflect ecophysiological adaptations to nutrient availability and salinity along the Shark River estuary (SRE), South Florida, USA. Linear models between leaf wax $\delta^{13}C_{n\text{-alkane}}$ values and species location along TP fertility and salinity gradients showed distinct differences, particularly between the species *A. germinans* and *R. mangle*. Our analyses showed that leaf wax $\delta^{13}C_{n\text{-alkane}}$ properly represented major differences in ecophysiological responses by each mangrove species. We also found that both *R. mangle* and *L. racemosa* showed different isotopic footprints among the SRE upper, middle and lower estuarine salinity regions. Further, the green leaves bulk $\delta^{13}C$ values in *R. mangle* (−32.3‰ to −27.6‰) were positively correlated with distance from the mouth of the estuary. In contrast, *L. racemosa* showed a negative relationship with distance and a narrower bulk $\delta^{13}C$ range (−29.8‰ to −28.1‰) in comparison to the other two species. *A. germinans*, a species found only in the brackish (salinity: 18.8 ± 1.2) and saline (30.3 ± 0.53) estuarine regions, also showed a positive bulk $\delta^{13}C$ relationship with distance. Because of the well-defined species-specific leaf wax *n*-alkane $\delta^{13}C$ values along both water column/soil pore water salinity and TP gradients, we propose these values as a potential salinity proxy for paleoclimate reconstruction.

1. Introduction

Plants living in terrestrial and coastal environments show unique stable carbon and nitrogen isotope values (i.e., $\delta^{13}C$ and $\delta^{15}N$) that are apparently the results of pulsing (e.g., nutrient enrichment) or incremental long term (e.g., CO_2 concentration) changes along environmental gradient regulating both plant productivity trends and ecophysiological responses (e.g., Cloern et al., 2002; Werner and Schnyder, 2012). This isotopic signature emerges either by the effect of a single environmental variable or a set of different variables according to their specific inter-annual and seasonal variability, including anthropogenic impacts (Dawson and Siegwolf, 2011). Moreover, characterizing and utilizing proxy integrative measures of ecosystem function, such as carbon and nitrogen isotope signatures (e.g., ecological stoichiometry) represents one of the most promising strategies to evaluate how plant communities respond to changes in environmental drivers at the local, regional and global scale (Sterner and Elser, 2002). In fact, one of the major research questions is how environmental drivers including seasonal and inter-annual variation magnify or alleviate environmental stress, for example, on plant growth and colonization/expansion, and how these processes are characterized in observed differences in plant bulk and compound-specific isotopic values (e.g., bulk $\delta^{13}C$ and $\delta^{15}N$, *n*-alkane $\delta^{13}C$; Diefendorf and Freimuth, 2017; McCarroll and Loader, 2004).

* Corresponding author.
E-mail address: vhrivera@lsu.edu (V.H. Rivera-Monroy).

https://doi.org/10.1016/j.ecss.2020.106768
Received 24 November 2019; Received in revised form 21 March 2020; Accepted 13 April 2020
Available online 18 April 2020
0272-7714/Published by Elsevier Ltd.

Mangrove wetlands dominate tropical and subtropical coastlines and therefore experience a wide range of fluctuating environmental conditions in coastal regions. Given the spatial distribution of this type of forested wetlands across a wide range of latitudes and coastal environmental settings, mangrove forests are an excellent system to test hypotheses about how individual plant species isotopic signatures respond to fluctuating environmental changes (i.e., stressful vs. benign) at different spatiotemporal scales (Rivera-Monroy et al., 2017). Mangrove wetlands net primary productivity (NPP) is among the highest in the world (range: 5–20 t dry weight ha^{-1} yr^{-1}; Alongi, 2009), and along with forest structure, it is controlled by the dynamic interaction among macroclimatic drivers (e.g., temperature, precipitation), resources (e.g., nitrogen, phosphorus), regulators (e.g., salinity, sulfide) and hydroperiod (e.g., flooding frequency and duration; Twilley and Rivera-Monroy, 2009; Twilley et al., 2019). Because of stressful environmental conditions, plant diversity in mangrove-dominated ecosystems is low when compared to other ecosystems (e.g., tropical and boreal forests) since plants require adaptations to cope with extremes changes including high soil salinity (>50), sulfide (H_2S; >1 μM), nutrient limitation (e.g., phosphorous) and high flooding duration and frequency (Rivera-Monroy et al., 2017). Thus, mangrove species variability at local scales is well represented by species zonation along well-defined fertility gradients, productivity levels, carbon sequestration rates in response, for instance, to pressing (e.g., tidal cycle) or pulsing (storm surge) flooding regimes (Rivera-Monroy et al., 2017; Rovai et al., 2016; Simard et al., 2019).

Although salinity has been identified as a key stressor affecting mangrove plants photosynthetic rates and nutrient uptake, it is not clear how other stressors (e.g., H_2S), resources (e.g., phosphorus, nitrogen) and hydroperiod interact to control carbon balance at the plant and forest stand level (e.g., Bouillon et al., 2011, 2008; Troxler et al., 2013). This interaction is reflected in mangrove species $\delta^{13}C$ and $\delta^{15}N$ isotopic values in leaves where light absorption, CO_2 uptake, and water exchange take place (Ball, 1988, 2002; López-Hoffman et al., 2006; Lovelock et al., 2006; Schmitz et al., 2006). Further, NPP, controlled by photosynthesis and coupled with nutrient availability, could significantly affect $\delta^{13}C$ signatures (Lin and Sternberg, 1992a,b; McKee et al., 2002; Rivera-Monroy et al., 2019; Sun et al., 1996). Additionally, since leaf wax components such as *n*-alkanes are preserved in mangrove soils (Diefendorf et al., 2010), their $\delta^{13}C$ values could be used not only to capture the environmental variability in present conditions, but also to serve in paleoecological and paleoclimatic studies on the response of mangroves to environmental change including sea-level rise (Webb et al., 2013; Yao et al., 2015). Specifically, prior studies have shown a relationship between the hydrogen isotopic composition of *n*-alkanes and salinity (He et al., 2017) that along with $\delta^{13}C_{n\text{-alkane}}$ values could provide further evidence and information on the role of environmental stressors in mangrove-dominated ecosystems (Ladd and Sachs, 2013).

In this study, we evaluated spatial differences in mangrove leaf wax $\delta^{13}C_{n\text{-alkane}}$ and bulk $\delta^{13}C/\delta^{15}N$ values along the Shark River estuary (SRE), a subtropical, mangrove-dominated estuary in South Florida (Everglades), USA. Because this coastal region is characterized by a wide range in mangrove tree height (average range: 2–18 m; Simard et al., 2006) and NPP (5–8 Mg C ha^{-1} yr^{-1}; Danielson et al., 2017) along distinct pore water salinity and soil total phosphorus (TP) fertility gradients (e.g., Castañeda-Moya et al., 2020) the SRE provides an ideal setting to assess the spatial variation in both leaf $\delta^{13}C_{n\text{-alkane}}$ and bulk isotope values (i.e., $\delta^{13}C$ and $\delta^{15}N$) in mangrove forests. Here, we addressed the following research questions: 1) what is the relationship between soil nutrient fertility and salinity gradients and mangrove species-specific C_{31} *n*-alkane $\delta^{13}C$ ($\delta^{13}C_{31}$) content in green leaves? and 2) are there a significant difference in brown-senescent leaves C:N ratios among sites and how do these differences compare with spatial differences in $\delta^{13}C_{31}$ among species? We hypothesized that given the ecophysiological differences among the mangrove dominant species, the $\delta^{13}C_{31}$ enrichment would be distinct among species regardless of location along the estuary.

2. Materials and methods

2.1. Study sites and sample collection

The Shark River estuary (SRE) is located in the southwest region of the Florida Coastal Everglades, Florida USA (Fig. 1). It is characterized by diurnal tides with a mean amplitude of 0.5–1.0 m in the southwestern region (Wanless et al., 1994). The dominant plant species in this oligohaline Everglades Mangrove Ecotone Region (EMER) are mangrove forests (Rivera-Monroy et al., 2011; Simard et al., 2006), ranging in average tree height from 5 to 18 m and generally decreasing with distance inland (Castañeda-Moya et al., 2013). The dominant mangrove species are *Rhizophora mangle*, *Laguncularia racemosa*, and *Avicennia germinans* (Danielson et al., 2017). Mangrove forest structure and NPP are directly related to well-defined soil salinity and soil TP gradients along the SRE (Castañeda-Moya et al., 2020; Rivera-Monroy et al., 2019). The highest soil pore water salinity and TP values are observed close to the mouth of the SRE while the lowest are registered upstream (salinity range: 4–30; TP: 0.12–0.23 mg cm^{-3}). As a result of this difference in soil phosphorus availability, forest NPP is higher downstream close to the mouth than upstream. Other sources of inorganic nutrients are subsurface flow and groundwater derived from upstream freshwater flushing (Rudnick et al., 1999).

We collected mangrove green leaves from the three dominant mangrove species along this salinity and fertility gradients along the SRE. Green leaves of the species *L. racemosa*, *R. mangle*, and *A. germinans* were collected from 11 sites on March 13–14 2013 (Table S1; Fig. 1). Sites S#2, S#5, and S#8 (Fig. 1) correspond to mangrove sites that are part of the sites network established by the Florida Coastal Everglades Long Term Ecological Research (FCE-LTER) program since 2001 (Childers, 2006; http://fcelter.fiu.edu/) and where long-term structural and productivity studies have been performed during the last 15 years (i.e., S#2 = *SRS-4*, S#5 = *SRS-5*, and S#8 = *SRS-6*; Danielson et al., 2017). Multiple green leaves (sun leaves) were collected by hand using surgical gloves from a randomly selected tree and immediately placed in a Ziploc bag, stored in a cooler with ice (temperature, −4 °C) and transported to the laboratory the same day of collection where they were stored in a freezer (temperature, −20 °C) until isotopic analysis (see below). The surface water salinity was measured in the adjacent estuarine water column at each site at the time of plant material collection using a YSI Proplus sonde (YSI California, USA). To evaluate the relationship between both the compound-specific isotopic values and carbon and

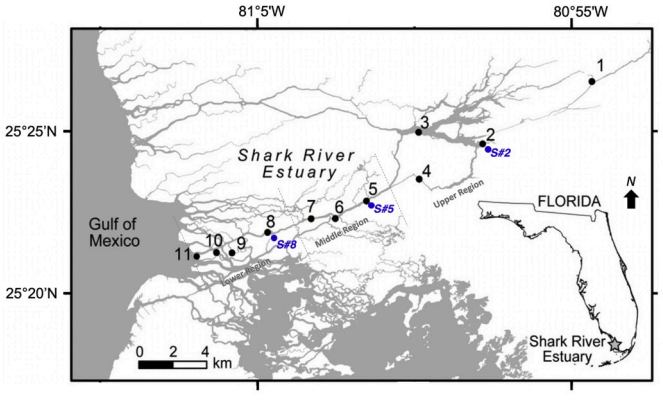

Fig. 1. Map of the Shark River estuary, South Florida. Sampling sites are marked with bold numbers from downstream (11) to upstream (1). Discrete sites where brown-senescent leaves were collected monthly in 2013 are in blue color. Soluble reactive phosphorus was also collected in S#8, S#5, and S#2 in the dry and wet seasons (2013). (For interpretation of the references to color in this figure legend, the reader is referred to the Web version of this article.)

nitrogen ratios with surface water salinity values, the sampling stations were spatially grouped into three regions: upper (sites S1–S4), middle (sites S5–S7), and lower (sites S8–S11) (Fig. 1).

In addition to the collection of green leaves in March 2013, we also monthly sampled brown-senescent leaves in litterfall baskets from January to December 2013. For further experimental design details about this monthly sampling, see Castañeda-Moya et al. (2013) and Danielson et al. (2017). Briefly, litterfall was collected in five 0.25 m^2 baskets (i.e., sampling units) within two 20 m × 20 m plots (i.e. replicates) established in sites S#2, S#5 and S#8 (Fig. 1) (10 baskets per site; 5 baskets per plot); these sampling sites and plots are part of the FCE-LTER sites (Childers, 2006). The baskets were positioned 1.5 m above ground and lined with 1 mm mesh screening. Litterfall from each basket was sorted and weighed by leaf species. Dry leaf material per species was combined per plot and site prior to chemical analysis (see below).

2.2. Analytical methods

2.2.1. Bulk green leaf $\delta^{13}C$ and $\delta^{15}N$ measurements

Entire green leaves were used for extraction to ensure integration of the signal from the leaf, avoiding possible isotopic differences along leaf length (Gao and Huang, 2013). All the samples were freeze-dried at −50 °C, and then shredded to a fine powder using a clean pair of scissors and a mortar. The bulk $\delta^{13}C$ and $\delta^{15}N$ values were measured using standard elemental analysis-isotope ratio mass spectrometry (EA-IRMS; Delta V, Thermo fisher, USA) and were reported with respect to the Vienna Peedee Belemnite (VPDB) standard and atmospheric nitrogen, respectively (Anderson and Fourqurean, 2003; Coplen et al., 1983). The precisions of bulk $\delta^{13}C$ and $\delta^{15}N$ measurements were ±0.10‰ and 0.20‰, respectively, for all samples.

2.2.2. Green leaves n-alkane extraction and quantification

The aliphatic hydrocarbons fraction, containing the *n*-alkanes, was isolated and analyzed using the methods described in (He et al., 2015a, b). Briefly, freeze-dried samples were subjected to sonication extraction 3x (0.5 h each) with high purity CH_2Cl_2 (Optima, Fisher, USA) as the solvent. After concentrating, the three extracts were combined and fractionated by adsorption chromatography over silica gel. Aliphatic hydrocarbons were eluted using *n*-hexane, as described by (He et al., 2014, 2015b). Randomly selected Ziploc bags used for leaf sampling and transport were pre-washed with *n*-hexane to assess potential sample cross-contamination. Results indicated no significant contamination (data no-shown).

A gas chromatography-mass spectrometry (GC-MS; GC-MS; Hewlett-Packard 5973, USA) system was used for the identification and semi-quantification of *n*-alkanes. The capillary column was a DB-1 MS (30m, 0.25 mm i.d., 0.25 μm film thickness; Agilent). The GC oven was programmed from 60 to 300 °C at a rate of 6 °C per min after 1 min at the initial temperature and then kept at the maximum temperature for 20 min. All *n*-alkanes were identified by 1) comparison of mass spectra to NIST 2008 library (e.g., He et al., 2018), 2) comparison with authentic standards and by 3) GC retention characteristics. A known amount of squalene was added to the aliphatic hydrocarbon fraction as an internal standard for semi-quantitative analysis (He et al., 2014).

2.2.3. $\delta^{13}C$ compound specific carbon isotope analysis

The aliphatic hydrocarbon fraction was analyzed to obtain the $\delta^{13}C$ values for all the *n*-alkanes, as described by He et al. (2016, 2015b). Briefly, compound-specific $\delta^{13}C$ values of *n*-alkanes were measured using a gas chromatography-isotope ratio mass spectrometry (GC-IRMS) system (Thermo, USA, consisting of a Thermo Trace GC Ultra (Thermo, USA) system equipped with a DB-1 fused silica capillary column (30 m long, 0.25 mm ID, 0.25 μm df), a Thermo GC/TC 2 interface (Thermo, USA), and a Thermo Delta V IRMS (Thermo, USA). The oven temperature for the conversion of compounds to CO_2 was held at 960 °C. The chromatographic conditions followed the procedure as described in section *2.2.2*. Three standards mixtures with known $\delta^{13}C$ values containing C17 *n*-alkane and squalane (different concentrations as 30 ng μL^{-1}, 200 ng μL^{-1}, and 500 ng μL^{-1}) were inserted between every four samples to check instrument performance, including linearity correction, if necessary. In addition, a known amount of squalane was also co-injected with samples as an internal standard for stable carbon isotopic measurements. The $\delta^{13}C$ values are given in per mil (‰) notation relative to the VPDB standard (Coplen et al., 1983). Error interval was estimated through the repeat analyses of selected samples (n = 3), yielding standard deviations within ±0.4‰; only compounds present in sufficient quantities for reliable $\delta^{13}C$ measurements (intensity above 1000 mVs) were used in the final interpretation of results.

2.2.4. Calculation of concentration-weighted average (CWA) leaf wax n-alkane $\delta^{13}C$ values ($\delta^{13}C_{27\text{-}33}$)

The C_{31} *n*-alkane, an abundant component in higher plant leaf waxes, was consistently measured to obtain $\delta^{13}C$ values, and used for comparison among the three Everglades mangrove species. Similarly, the CWA for long-chain leaf wax *n*-alkane $\delta^{13}C$ values ($\delta^{13}C_{27\text{-}33}$) were also calculated for each species using Eq. (1):

$$\delta^{13}C_{27-33} = \sum_{k=27}^{33} \frac{\delta 13Ck \times Conc.k}{Con.tot} \quad (1)$$

where $\delta^{13}Ck$ is $\delta^{13}C_{27} - \delta^{13}C_{33}$ (only odd carbon number homologues), $Conc._k$ is the concentration of *n*-C_{27} – *n*-C_{33} alkanes (only odd carbon number homologues) in μg g^{-1} dry weight (μg gdw^{-1}) leaf material and $Conc._{tot}$ is the total concentration of *n*-C_{27} – *n*-C_{33} alkanes (only odd carbon number homologues). We included C_{27} *n*-alkane for the CWA calculation because of its relatively relative high abundance (27%–33% of total *n*-alkanes) in *L. racemosa*. We deliberately excluded *n*-alkanes below C_{27} because C_{23} and C_{25} in sediments could be primarily derived from other types of plants, especially submerged aquatic plants (Ficken et al., 2000; Mead et al., 2005), which might weaken applicability of the CWA proxy proposed here for sedimentary records. The C_{35} *n*-alkane was not included in this assessment due to its low concentration and inconsistent detection in many samples. These CWA isotopic values could facilitate comparison among species with different *n*-alkane composition and have been used in previous studies (e.g., Kahmen et al., 2013).

2.2.5. Calculation of apparent carbon isotopic fractionation factor

The net fractionation factor between the $\delta^{13}C$ values of CO_2 and the green bulk leaf or *n*-alkane was calculated using Eq. (2):

$$\alpha_{atm\text{-}leaf\ or\ n\text{-}alkane} = (^{13}C/^{12}C)_{atm}/(^{13}C/^{12}C)_{leaf\ or\ n\text{-}alkane} = (\delta^{13}C_{leaf\ or\ n\text{-}alkane} + 1000)/(\delta^{13}C_{atm} + 1000) \quad (2)$$

The $\delta^{13}C$ value of atmospheric CO_2 was averaged as −8.45‰ based on monthly average values during the year 2012 from Key Biscayne, Florida, USA; http://www.esrl.noaa.gov/gmd/dv/data/).

2.2.6. Brown-senescent leaves total organic carbon, organic nitrogen, and phosphorus concentrations

Both total organic carbon (OC) and nitrogen (ON) concentrations were determined on two analytical replicates of each composite brown-leaf material per plot with an ECS 4010 elemental analyzer (Costech Analytical Technologies, Inc., Valencia, California). Total phosphorus (TP) was determined by extraction on duplicate leaf sampling material with 1 N HCl after combustion in a furnace at 550 °C for 2 h (Aspila et al., 1976) and determined by colorimetric analysis using a segmented flow analysis Flow Solution IV autoanalyzer (OI Analytical, College Station, Texas).

2.2.7. Soil pore water salinity and soluble reactive phosphorus (SRP)

Salinity and soluble reactive phosphorus (SRP, PO_4^{-3}) concentrations

were measured in soil pore water at 30 cm depth in the dry (May) and wet (October) seasons (2013) in sites S#2, S#5, and S#8 (Fig. 1) as described in Castañeda-Moya et al. (2013). Briefly, within each site, four sampling stations were randomly established in each of the two litterfall plots. Water samples were collected using a rigid plastic probe (3/16" OD) attached to a suction device. One pore water aliquot was assayed for temperature and salinity using a portable YSI Proplus sonde (model 30, YSI Incorporated, Yellow Springs, Ohio). A second pore water sample was filtered using a GF/F filter and stored frozen until SRP analysis using a segmented flow analysis Flow Solution IV autoanalyzer (OI Analytical, College Station, Texas).

2.2.8. Statistical analyses

Statistical analysis was performed using SAS- JMP Pro 12 (SAS Institute, Cary, NC, USA) and SPSS 13.0 for Windows; SAS-JMP Pro was also used to prepare graphical material (Figs. 4–7). We performed linear regressions and factorial ANOVAS (fixed factors) to evaluate differences in carbon concentrations and isotopic values among estuarine regions, mangrove species and their interactions. The design was incomplete and unbalanced because not all species occurred at each site (i.e., *A. germinans*). A significant factor effect was followed by a Tukey's multiple-comparison test (Tukey HSD) and confidence intervals (95%) were included in the linear regressions. Data that did not meet normality or variance homogeneity assumptions were transformed, but the untransformed means (±1 SE) are presented.

3. Results

3.1. Water column and pore water salinity and SRP spatial distribution along the SRE

Water column salinity values along the SRE showed a distinct spatial pattern ($p < 0.0001$; MSE: 1867; $F_{2,27}$: 198.9; Table S2) with the lower values measured upstream (stations 1–4: 4.6 ± 1.0) and the highest at the mouth of the estuary (stations 8–11: 30.3 ± 0.7) while the brackish values were observed in the middle region (stations 5–7; 18.8 ± 1.2) (Figs. 1 and 2). Salinity values in pore water sampled in the dry and wet seasons (Fig. 3A) were similar to values reported for the same sites (stations: S#2, S#5, S#8) in previous years (i.e., Castañeda-Moya et al., 2013, 2010); these values followed the same trend as in the water column, with lower values upstream and higher values downstream (Fig. 2). The maximum pore water salinity value in 2013 was observed at station S#8 (20.7 ± 1.4) and the lowest (1.7 ± 1.18) upstream in station S#2 (Table S3; Fig. 3A) during the wet season; mean values between seasons were similar in stations S#5 and S#8 (Table S3).

Soil pore water SRP concentrations sampled in the dry and wet seasons were significantly different among sites S#8, S#5, and S#2 (Table S4; Figs. 1 and 3B). The highest mean value was measured in S#8 (1.81 ± 1.3 μM) and the lowest in S#2 (0.24 ± 1.18 μM; Fig. 3B). There was an interaction between site and season with significant differences between the dry and wet season only in S#5 (Table S4; Fig. 3B).

3.2. Mangrove leaf C, N and P content and C:N ratios

3.2.1. Green leaves

OC and ON percentage (%) and C:N atomic ratio values in green mangrove leaves showed significant differences between species and location along the estuary (Fig. 4A-C). The species *A. germinans* was absent upstream where the average water column (<4) and soil pore water salinity (<5) values were low. This species green leaf mean OC% values were higher in the middle region (57.3 ± 2.1) than in sites closer to the mouth of the estuary (51.0 ± 1.2) (Fig. 4A). This spatial pattern was similar in the case of *R. mangle* (middle: 57.6 ± 0.7; lower: 54.7 ± 1.4), although the lowest value was registered upstream where this species is the dominant species (53.1 ± 1.3) (Fig. 1; Fig. 4A). In contrast, the species *L. racemosa* had low mean values along the estuary (48.1–48.8, Fig. 4A).

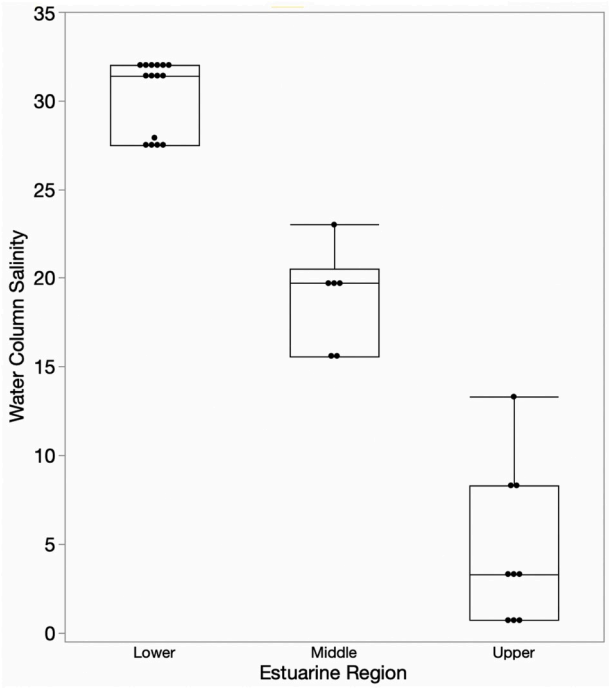

Fig. 2. Salinity differences per estuarine region along the Shark River estuary, Florida, USA. Sampling locations are shown in Fig. 1; see Table S1 for latitude/longitude information. Closed circles represent individual measurements in each region.

Mean ON% values also showed significant differences between mangrove species and estuarine regions, with the highest values measured in *A. germinans* green leaves, especially in the lower estuarine region (2.0 ± 0.1) (Fig. 4B). In the case of *R. mangle*, the highest mean ON% values were registered in the upper estuarine region (1.2 ± 0.1), which were significantly different from values measured in the lower and middle (0.9 ± 0.1) stations (Fig. 4B). *L. racemosa* values were similar to those of *R. mangle*, with the exception of the middle estuarine region where the value was 0.7 ± 0.1 (Fig. 4B). C:N ratios were significantly lower for *A. germinans* (26.0–43.0) that in the case of *R. mangle* (46.1–62.4) and *L. racemosa* (47.9–67.0) (ANOVA; MSE = 1719.9, F = 12.2, $p = 0.0001$) (Fig. 4C) reflecting the systematic high ON% in *A. germinans* green leaves (Fig. 4B).

3.3. Brown-senescent leaves

Average OC% and ON% and C:N atomic ratio values in brown senescent leaves sampled monthly (2013) in sites S#2 (upstream), S#5 (middle), and S#8 (downstream) (Figs. 1, 4D-F) show differences when compared with green leaf values (Fig. 4A–C). Whereas brown leaf OC% values were similar among sites and species (range: 44.4–45.2; Fig. 4D), green leaves showed a significant interaction between species and location (Fig. 4A). The overall average ON% in brown leaves (Fig. 4E), were higher close to the estuary mouth (site S#8; 0.93 ± 0.02) than in sites S#5 (0.70 ± 0.02) and S#2 (0.57 ± 0.01; this gradient followed the same pattern as that for the green leaves (Fig. 4B), but mean values were lower. Brown-senescent leaves C:N (atomic) ratio showed distinct spatial patterns across all sites; the highest values were registered upstream for the *R. mangle* and *L. racemosa* species (Fig. 4F). On average, all C:N atomic ratios were higher in the brown-sencescent leaves than in green leaves (Figure C).

Brown-senescent leaves TP concentrations among species within sites were significantly different (Table S5). Mean concentrations were similar among species in sites S#5 and S#2, but significantly different in

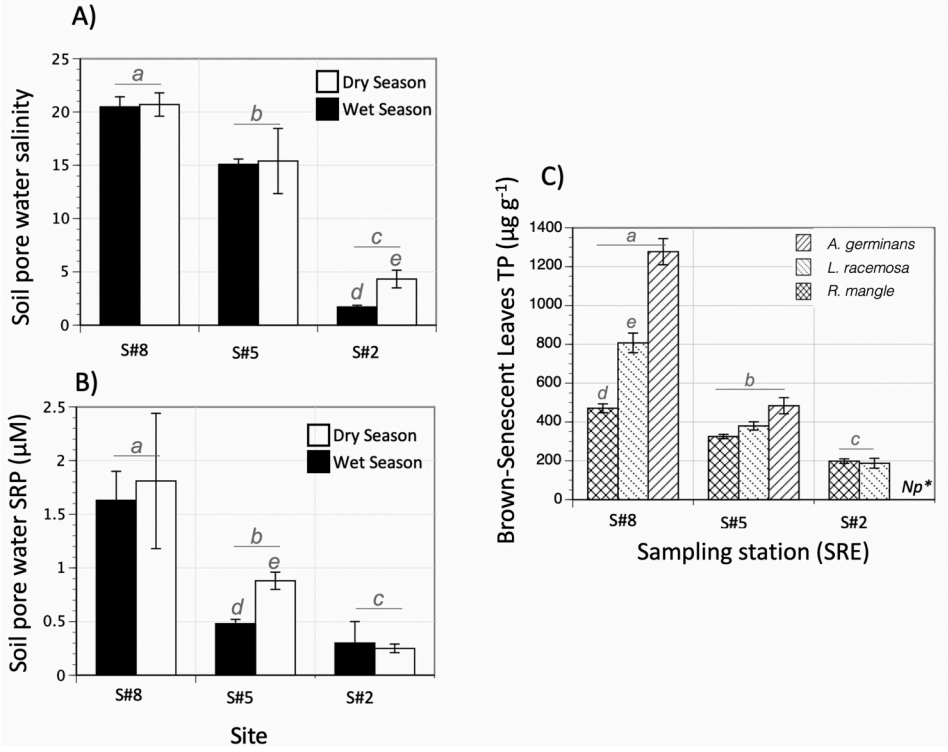

Fig. 3. Pore water physicochemical variables: A) salinity; B) soluble reactive phosphorus (SRP; PO_4^{-3}, μM) in three stations along the Shark River Estuary (SRE): S#8, Lower; S#5, Middle; S#2, Upper. C) Total phosphorus (TP) in brown-senescent leaves (μg gdw^{-1}). *Np** = species is no present. Different letters indicate significant differences ($p < 0.001$) across sites and species. ANOVA results are in Table S2. (For interpretation of the references to color in this figure legend, the reader is referred to the Web version of this article.)

the case of site S#8 (Fig. 3C). *L. racemosa* (168.6 ± 17.8 μg gdw^{-1}) and *R. mangle* (196.0 ± 11.5 μg gdw^{-1}) show low concentrations in site S#2 (Table S5; Fig. 3C). The highest leaf TP concentration in site S#8 was observed in brown leaves of the species *A. germinans* (1301.1 ± 65.6 μg gdw^{-1}) and the lowest in *L. racemosa* (470.6 ± 22.8 μg gdw^{-1}) at S#2; overall, the site S#8 has the highest mean TP concentration (849.8 ± 7.3 μg gdw^{-1}) across all sites (Fig. 1; Fig. 3C; Table S5).

3.4. Bulk green leaf $\delta^{13}C$ and $\delta^{15}N$ values among mangrove species

Green leaves bulk $\delta^{13}C_{leaf}$ values ranged from −32.3 to −27.8‰ for the three mangrove species: *R. mangle*: −32.3 to −27.8‰ (range: 4.5‰); *L. racemosa*: −29.8 to −28.1‰ (range: 1.7‰) and *A. germinans*: 31.4 to −28.5‰ (range: 2.9‰) (Table S1; Fig. 5A), with the most narrow range observed for *L. racemosa* (Table S1). All species show a conspicuous spatial relationship between distance from the mouth of the estuary and bulk $\delta^{13}C$ enrichment values; this distance is associated with changes in both water and soil pore water salinities and SRP (Figs. 2 and 3A, B). A positive linear relationship was observed in the case of *A. germinans* (RMSE = 0.77; $R^2 = 0.612$; $p < 0.02$) and *R. mangle* (RMSE = 1.03; $R^2 = 0.665$; $p < 0.002$) in contrast to the species *L. racemosa*, which showed a significantly (RMSE = 0.39; $R^2 = 0.52$; $p < 0.01$) negative relationship, although with a lower slope (i.e., b = 0.05) (Fig. 5A).

Bulk green $\delta^{15}N$ spatial trends also showed significant relationships between species and estuarine salinity gradients. In this interaction, the overall linear trend for *L. racemosa* (RMSE = 1.32; $R^2 = 0.646$; $p < 0.005$) and *R. mangle* (RMSE = 0.61; $R^2 = 0.767$; $p < 0.001$) were similar with the most depleted bulk $\delta^{15}N$ values observed in the upper, fresher estuarine region (Fig. 5B). In the case of the *L. racemosa*, we observed two distinct groups with the lowest mean enrichment (1.85 ± 0.47) in the upper region (Fig. 5B). This was also the case for the species *R. mangle* where low mean depleted values were measured in the freshwater region (2.05 ± 0.38) while the enriched values were observed in both the brackish (3.73 ± 0.54) and saline (3.80 ± 0.38) estuarine regions (Fig. 5B); no significant relationship between the saline and brackish regions was observed in the case of *A. germinans* (RMSE = 0.65; $R^2 = 0.046$; $p < 0.60$) (Fig. 5B). Additionally, we observed significant differences in the relationship between $\delta^{13}C$ and $\delta^{15}N$ (Fig. 5C), where a positive linear relationship was registered in the case of *L. racemosa* (RMSE = 1.49; $R^2 = 0.548$; $p < 0.01$), in contrast to a negative relationship in the case of *R. mangle* (RMSE = 0.99; $R^2 = 0.395$; $p < 0.01$). As in the case of the spatial variability of bulk $\delta^{15}N$ (Fig. 5B), the species *A. germinans* did not show differences in the relationship between $\delta^{13}C$and $\delta^{15}N$ (RMSE = 0.65; $R^2 = 0.025$); $p < 0.70$) (Fig. 5C).

3.5. Bulk green leaves wax n-alkane $\delta^{13}C$ values

All $\delta^{13}C_{n\text{-alkane}}$ green leaves values were significantly more depleted (Fig. 6A and B) than their corresponding bulk green $\delta^{13}C_{leaf}$ values (Fig. 5A and B) as observed in other vascular plants (Diefendorf et al., 2011). The C_{31} *n*-alkane $\delta^{13}C$ ($\delta^{13}C_{31}$) values in green leaves ranged from −41.8 to −35.7‰ (*R. mangle*; range: 6.1‰), −38.2 to −35.5‰ (*L. racemosa*; range: 2.7‰) and −36.9 to −34.1‰ (*A. germinans*; range: 2.8‰) (Fig. 6B). The net fractionation from atmospheric CO_2 to C_{31} *n*-alkane, $\alpha_{atm\text{-}C31}$ (calculated using Eq. (2)) ranged from 0.968 to 0.972 (*R. mangle*), 0.970 to 0.973 (*L. racemosa*), and 0.971 to 0.974 (*A. germinans*). Overall, both *A. germinans* and *L. racemosa* species have significantly more enriched $\delta^{13}C_{31}$ values compared to those measured for *R.mangle*, especially in the saline and brackish estuarine regions (Fig. 6A and B). Enriched $\delta^{13}C_{31}$ values and linearly correlated with changes in salinity; this relationship is positive in the case of *A. germinans* (Y = −36.15 + 0.2549*X, $p < 0.04$) and *R. mangle* (Y = −40.72 + 0.1687*X, $p < 0.001$) and negative in the case of *L. racemosa* (Y = −36.63 + 0.09818*X, $p < 0.003$; Fig. 6B). These values are within the range of observed values in angiosperm plant leaves (ca. 10‰ and 8.5‰ for $\delta^{13}C_{31}$ (Diefendorf et al., 2011). As in the case of the bulk $\delta^{13}C_{leaf}$ values, the wax $\delta^{13}C_{n\text{-alkane}}$ (C_{27-C33}) values also follow similar spatial patterns where a negative relationship was observed along the estuary for *L. racemosa* (Y = 36.06–0.1563*X, $p < 0.008$; Fig. 6A) in contrast to a positive spatial association in the case of *R. mangle* (Y = −40.13 + 0.1126*X, $p < 0.0002$; Fig. 6A). In the case of the species *A. germinans*, a significant linear relationship was also observed (Y =

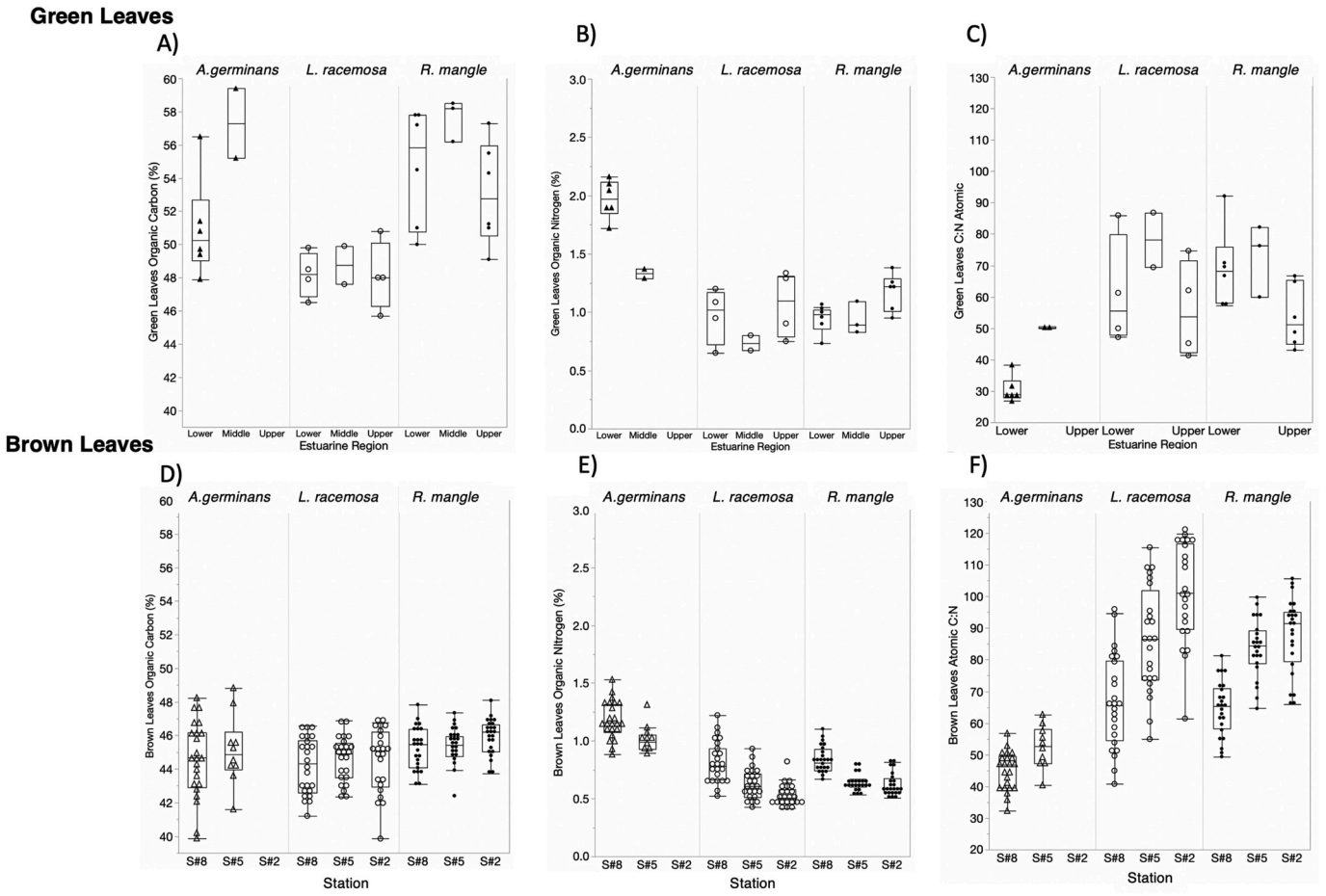

Fig. 4. Canopy green and brown leaves organic carbon and nitrogen percentage and C:N (atomic) ratios of the three mangrove species sampled along the Shark River estuary. Green leaves: A) organic carbon (%), B) organic nitrogen (%), C) C:N ratio (atomic); Brown-senescent leaves: D) organic carbon (%), E) organic nitrogen (%), F) C:N ratio (atomic). Stations S#2, S#5, and S#8 are located in the lower, middle and upper eEstuarine region, respectively (see Fig. 1). Triangles and circles in the box plots represent individual observations (see methods for details). (For interpretation of the references to color in this figure legend, the reader is referred to the Web version of this article.)

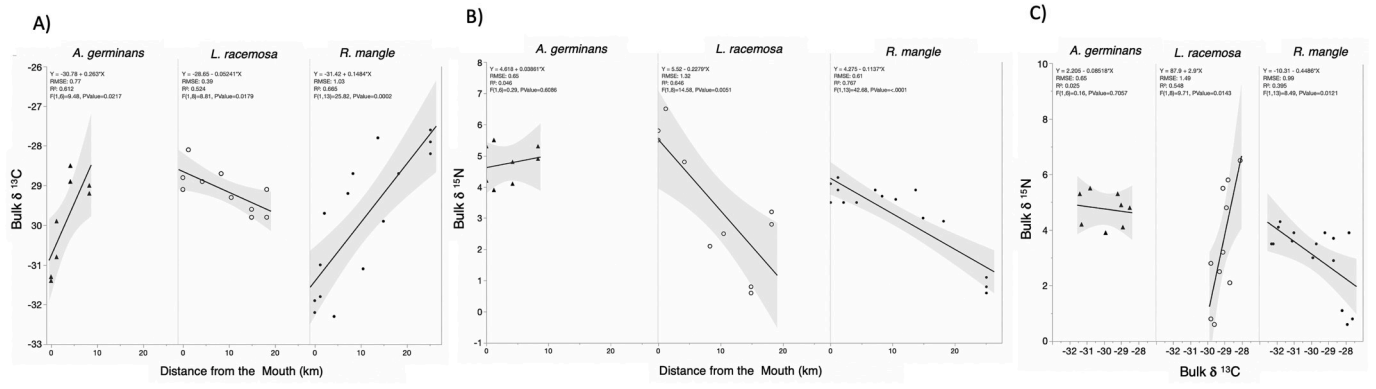

Fig. 5. Mangrove green leaves A) bulk $\delta^{13}C$ and B) bulk $\delta^{15}N$ values for each mangrove species (*A. germinans, L. racemosa, R. mangle*) within Shark River estuarine regions; C) relationship between bulk $\delta^{13}C$ and bulk $\delta^{15}N$ values per species. The grey band shows the 95% confidence interval. (For interpretation of the references to color in this figure legend, the reader is referred to the Web version of this article.)

$-37.7 + 0.2571*X$, $p < 0.02$; Fig. 6A).

4. Discussion

4.1. Bulk green leaves $\delta^{13}C$ and $\delta^{15}N$ and wax n-alkane $\delta^{13}C$ values

Our analyses of bulk OC/ON isotopes and leaf wax *n*-alkane $\delta^{13}C$ values in green leaves showed linear relationships among species spatial distribution, soil TP fertility, and salinity (water column and soil pore water) in the SRE; this relationship was also observed for the brown-senescent leaves C:N atomic ratios of the mangrove species *A. germinans*, *L. racemosa*, and *R. mangle*. Based on previous work (Fry et al., 2000; Mancera-Pineda et al., 2009), we hypothesized that given the ecophysiological differences among the dominant mangrove species,

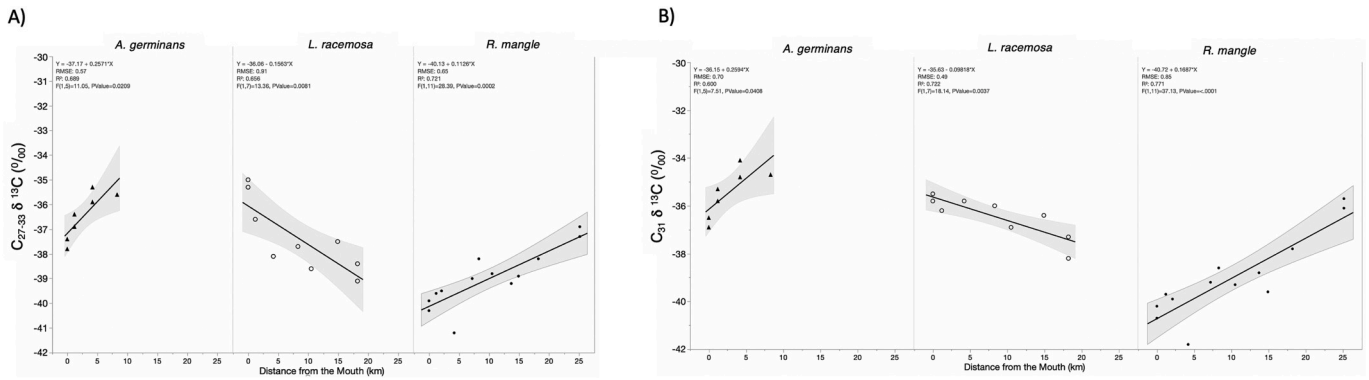

Fig. 6. Mangrove green leaves wax *n*-alkane $\delta^{13}C$ values per mangrove specie along the Shark River estuary. A) $\delta^{13}C_{n\text{-alkane}}$ (C_{27-C33}); B) $\delta^{13}C_{n\text{-alkane}}$ (C_{31}). The grey band shows the 95% confidence interval. (For interpretation of the references to color in this figure legend, the reader is referred to the Web version of this article.)

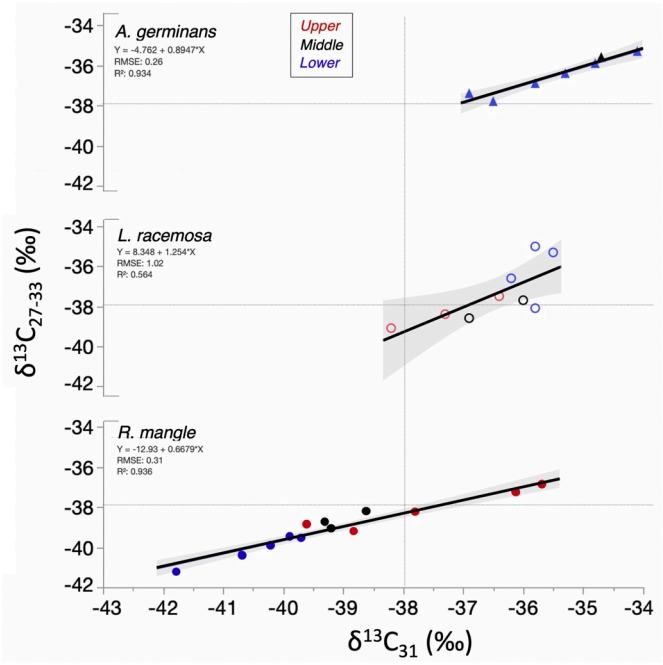

Fig. 7. Relationship between mangrove green leaves wax $\delta^{13}C_{27\text{-}33}$ and $\delta^{13}C_{31}$ values for each mangrove species. Colors indicate regions along the Shark River estuary (see Fig. 1). The grey band shows the 95% confidence interval. (For interpretation of the references to color in this figure legend, the reader is referred to the Web version of this article.)

the $\delta^{13}C$ values would be distinct among species regardless of location. Indeed, we not only found that each species has a characteristic range of values, but also that the magnitude is associated to species relative density in each estuarine region associated to both salinities (water column and soil pore water) and soil TP concentrations. This pattern is evident in the case of *R. mangle*, which is a species present in all sites with variable tree density showing a broader range in green leaves $\delta^{13}C_{31}$ values than *L. racemosa* and *A. germinans* (Fig. 7).

Because *n*-alkanes are known to be stable on geological timescales of up to millions of years and therefore widely used in paleoclimatic studies (e.g., Diefendorf et al., 2010), we explored if the observed trends on compound-specific $\delta^{13}C$ values correlate with those of the bulk stable carbon isotopes along the SRE. Although bulk organic matter $\delta^{13}C$ values can change during degradation, lipids such as long-chain *n*-alkanes, are more stable and reliable proxies for paleo-vegetation and paleoclimate studies (Eglinton and Eglinton, 2008; Meyers, 2003; Rao et al., 2009). To the best of our knowledge, only one study has investigated leaf wax $\delta^{13}C_{n\text{-alkane}}$ values spatial distribution in mangrove wetlands (Ladd and Sachs, 2013). This study, performed in the Brisbane River estuary, Australia, observed a significant positive correlation between salinity and leaf wax $\delta^{13}C_{n\text{-alkane}}$ values in leaves of the species *Avicennia marina*; but, matching our results only for *L. racemosa* (Fig. 6). In contrast, positive correlations between distance to the estuarine mouth and $\delta^{13}C_{n\text{-alkane}}$ values (or negative correlations between salinity and $\delta^{13}C_{n\text{-alkane}}$ values) were observed for *R. mangle* and *A. germinans*. We propose that given the covariation between both green bulk leaf $\delta^{13}C$ values and $\delta^{13}C_{n\text{-alkane}}$, this relationship could be used as a proxy for paleo-studies in mangrove dominated-ecosystems. In fact, our analyses showed that green leaves wax $\delta^{13}C_{31}$, although lower in value compared to bulk green leaves $\delta^{13}C$ value (Fig. 6), properly reflected the major differences in ecophysiological responses by each species to environmental gradients along the SRE (Fig. 6).

The significant linear relationships between salinity and $\delta^{13}C$ values –for both bulk and $\delta^{13}C_{31}$ along the SRE (Figs. 6 and 7)– indicate that stable carbon isotopes in mangrove wetlands can be influenced by salinity gradients, and thus may be used as indicators for the reconstruction of paleo-salinity regimes. Indeed, our results support the hypothesis that $\delta^{13}C_{n\text{-alkane}}$ in mangroves respond to environmental gradients, including salinity (Ladd and Sachs, 2013). Yet, it is essential to qualify this relationship in the case of bulk leaf $\delta^{13}C$ values. Since $\delta^{13}C_{n\text{-alkane}}$ spatial patterns could be different among species in habitats with mixed mangrove species and where vegetation succession occurs at different temporal scales as a result of hurricane impacts, the use of $\delta^{13}C_{n\text{-alkane}}$ for paleosalinity reconstruction should be approached with caution. Nevertheless, the use of the $\delta^{13}C_{n\text{-alkane}}$ values as a salinity proxy in combination with traditional paleoecological studies using pollen to reconstruct past climates and vegetation structure (e.g., Yao et al., 2015) could provide valuable environmental change information in mangrove-dominated coastal regions. Still, further studies are needed to determine the changes in $\delta^{13}C_{n\text{-alkane}}$ values as green leaves become senescent, including the potential differences in values when senescent leaves start to be incorporated in the soil matrix as indicated by the gradual differences we observed between OC% and C:N ratio between green and senescent leaves (Fig. 4).

4.2. Species dominance along the salinity and TP fertility gradient and green leaves bulk $\delta^{13}C$ and $\delta^{15}N$ differences

Although the site and species differences in both green leaves bulk leaf $\delta^{13}C$ and $\delta^{15}N$ values are explained by a salinity gradient (i.e., a regulator; water column and soil porewater), it is also critical to consider the conspicuous soil TP fertility gradient (i.e., a resource) along the estuary. This spatial and temporal covariation of salinity and phosphorus fertility is of particular importance in our study sites given the role of natural disturbances in periodically fertilizing mangrove

wetlands as a result of storm surge deposition of mineral sediments rich in phosphorus (Ca–P bound); this mechanism enhances plant P uptake, as reflected in the brown-senescent leaves TP concentrations, and consequently NPP (Castañeda-Moya et al., 2020, 2010; Rivera-Monroy et al., 2019). Specifically, mangrove NPP differences along the SRE have been shown to be driven by differences in soil TP availability linked to both changes in estuarine and soil pore water salinity (Danielson et al., 2017; Rivera-Monroy et al., 2019). This direct relationship has been invoked as critical interaction regulating carbon dynamics (i.e. carbon sequestration and storage; Bouillon et al., 2008; Rivera-Monroy et al., 2013, 2019), especially the spatial-temporal differences in $\delta^{13}C$ values. The monthly leaf litterfall data for 2013 showed how brown-senescent leaves TP concentrations in all mangrove species significantly decrease from downstream (S#2) to upstream (S#8) (Fig. 3C) indicating how soil inorganic nutrient availability can both limit NPP and therefore influence green leaves $\delta^{15}N$ and $\delta^{13}C$ and leaf wax *n*-alkane $\delta^{13}C_{n\text{-alkane}}$ values in the long term. The TP enrichment in brown leaves in 2013 along the SRS has been also reported for other years (2008, 2014, 2018), especially few weeks after hurricane impacts (Castañeda-Moya et al., 2020).

Other mangrove isotopic studies assessing the spatial variability in bulk leaf $\delta^{15}N$ and $\delta^{13}C$ values have also reported the relative role of nutrient availability on the interaction with these isotopic values. For instance, one study in the Caribbean (Belize: McKee et al., 2002) indicated that spatial differences in $\delta^{15}N$ values "disappeared" when *R. mangle* mangrove trees were fertilized with P (fertilizer, P_2O_5) when growing under nitrogen and TP limitation. This change was explained by variations in P concentration that increased nitrogen demand and decreased fractionation (McKee et al., 2002). This study also found that the spatial reduction in $\delta^{13}C$ values in *R. mangle* green leaves was associated to an intrinsic P limitation in *R. mangle* scrub forest (tree stature < 3 m), where values were around −26.4‰, suggesting a spatial variation in environmental stresses controlling either stomatal conductance or carboxylation. These mechanisms might be similar in the case of the SRE, where the tallest trees (>15 m), growing under high TP availability, are found in the lower estuary while low tree stature (<5 m) is dominant in the upper region where both salinity (<4) and TP soil concentration (<0.12 mg cm^{-3}) are low. Indeed, we observed such a reduction in the $\delta^{13}C$ range with an enriched value around −28‰ in the upper region and values < −31‰ in the lower estuary, especially in the case of the species *R. mangle* and *A. germinans* (Fig. 5A). In the case of *L. racemosa*, Mancera-Pineda et al. (2009) also reported lower $\delta^{13}C$ values upstream (−30.4‰) versus downstream (−29.8‰) along the SRE, which followed the same trend we observed for this species, although these authors reported lower $\delta^{13}C$ values overall (Fig. 5A). Furthermore, these authors found no significant difference in *A. germinans* $\delta^{13}C$ green leaves values between the middle (−30.3‰) and upper (−30.3‰) estuarine salinity regions (Mancera-Pineda et al., 2009).

We propose that the regionally smaller $\delta^{13}C$ range measured in *L. racemosa* leaves along the SRE (Fig. 5A) indicates that this species is better adapted to wider fluctuations in environmental changes in salinity and nutrient availability than *R. mangle,* and possibly, *A. germinans*. Especially given *L. racemosa* dominance and high NPP in areas where salinity is > 25 along the SRE (Rivera-Monroy et al., 2019) and that this species has been classified as a shade-intolerant with moderate tolerance to hypersaline conditions; although other field studies indicate that *R. mangle* and *A. germinans* are more tolerant of shading than *L. racemosa* (Ball, 1988; Roth, 1992). Even when both *L. racemosa* and *A. germinans* show less efficient water transport at shoot level, these species are more efficient in water use at the leaf level in comparison to *R. mangle* (Medina et al., 2015; Sobrado, 1999). Our observations along the salinity gradient suggest the same pattern, particularly in the case of *L. racemosa*, considering that this species grows rapidly in areas where salinity is the highest in the SRE and becomes dominant in areas after significant defoliation and tree mortality as a result of tropical storms (Danielson et al., 2017; Rivera-Monroy et al., 2019; Smith et al., 2009). More experimental plant isotopic ecophysiological field and mesocosm studies are needed to assess the coupling of the N, P and C cycling as regulated by stressors such as salinity to elucidate this highly dynamic interaction at the leaf and individual plant scales.

5. Conclusions

This study revealed distinct bulk and compound-specific stable isotope "footprints" in green leaves of the neotropical mangrove species *R. mangle*, *L. racemosa*, and *A. germinans* along salinity and total phosphorus soil fertility gradients in the SRE, South Florida, USA. Spatial and species-specific differences in inorganic nutrient sources are highlighted by both mangrove brown-senescent leaves total phosphorus (TP) concentrations and bulk $\delta^{13}C$ and $\delta^{15}N$ enrichment. This spatial difference also underscores previously reported distinct nitrogen and TP loading rates as a result of significant differences in hydroperiod, tidal incursion, and groundwater flow that can be impacted by pulsing storms (Castañeda-Moya et al., 2020). Green leaves bulk$\delta^{13}C_{leaf}$ values in combination with compound-specific ($\delta^{13}C_{n\text{-alkane}}$) values further revealed differences in species-specific ecophysiological adaptations (e.g., water use efficiency, carboxylation) regulating nutrients uptake (e.g., N, P) while dealing with soil stressors such as pore water salinity; especially, in the case of the species *L. racemosa* and *R. mangle*. Further, our results support the hypothesis that $\delta^{13}C_{n\text{-alkane}}$ values in mangroves significantly change in response to environmental gradients, including salinity. The most conspicuous strong association between $\delta^{13}C_{31}$ and $\delta^{13}C_{27\text{-}33}$ in our study sites were observed for *A. germinans* and *R. mangle*, which are strengthened across distinct salinity and TP availability gradients. Thus, since *n*-alkanes are known to be stable on geological timescales, their stable carbon isotope values can potentially be used in paleoecological salinity investigations. This approach could enhance the strength in such paleo-assessments previously suggested for stable hydrogen isotope composition of *n-alkanes* (He et al., 2017). Our study highlights how stable isotopic composition of mangrove leaves are determined by the interaction between nutrient availability (i.e., soil TP) and landscape-level disturbances (i.e., tropical storms), which modulates hydrology and salinity gradients at different spatiotemporal scales in the SRE.

Declaration of competing interest

The authors declare that they have no known competing financial interests or personal relationships that could have appeared to influence the work reported in this paper.

CRediT authorship contribution statement

Ding He: Conceptualization, Data curation, Formal analysis, Funding acquisition, Methodology, Investigation, Writing - original draft, Writing - review & editing. **Victor H. Rivera-Monroy:** Conceptualization, Data curation, Formal analysis, Funding acquisition, Methodology, Investigation, Writing - original draft, Writing - review & editing. **Rudolf Jaffé:** Conceptualization, Data curation, Formal analysis, Funding acquisition, Methodology, Investigation, Project administration, Writing - review & editing. **Xiaochen Zhao:** Data curation, Formal analysis, Methodology, Investigation, Writing - review & editing.

Acknowledgments

The authors appreciate the assistance of J.L. Breithaupt (University of South Florida, USF), J.M. Smoak (USF), and Rafael Travieso (Florida International University, FIU) for field collections, Edward Castañeda-Moya for data discussions (FIU), and P.M. Medeiros (University of Georgia) for valuable comments. The assistance of J. Harris and W.T. Anderson (FIU) during isotope measurements is highly appreciated. This

work was funded in part by the US National Science Foundation through the Florida Coastal Everglades LTER program (DEB-1237517). R.J. and D.H. acknowledge additional support through the George Barley Endowment and the Cristina Menendez Fellowship, respectively. D.H. also acknowledges funding from the National Science Foundation of China [41973070 and 41773098 to D. He] and the Hundred-Talent Program foundation [188020*194231701/008 and 188020-193810201/102 to D. He] at Zhejiang University. V.H.R.M acknowledges the partial support of the US Department of the Interior – South Central Climate Adaptation Science Center, Cooperative Agreement#G12 AC00002. We thank three anonymous reviewers for constructive comments on earlier versions of this manuscript. This is SERC contribution number 959 from the Southeast Environmental Research Center at Florida International University.

Appendix A. Supplementary data

Supplementary data to this article can be found online at https://doi.org/10.1016/j.ecss.2020.106768.

References

López-Hoffman, L., DeNoyer, J.L., Monroe, I.E., Shaftel, R., Anten, N.P., Martínez-Ramos, M., Ackerly, D.D., 2006. Mangrove seedling net photosynthesis, growth, and survivorship are interactively affected by salinity and light 1. Biotropica 38, 606–616.

Alongi, D., 2009. The Energetics of Mangrove Forests. Springer Science & Business Media.

Anderson, W.T., Fourqurean, J.W., 2003. Intra-and interannual variability in seagrass carbon and nitrogen stable isotopes from south Florida, a preliminary study. Org. Geochem. 34, 185–194.

Aspila, K., Agemian, H., Chau, A., 1976. A semi-automated method for the determination of inorganic, organic and total phosphate in sediments. Analyst 101, 187–197.

Ball, M.C., 1988. Salinity tolerance in the mangroves Aegiceras corniculatum and Avicennia marina. I. Water use in relation to growth, carbon partitioning, and salt balance. Funct. Plant Biol. 15, 447–464.

Ball, M.C., 2002. Interactive effects of salinity and irradiance on growth: implications for mangrove forest structure along salinity gradients. Trees (Berl.) 16, 126–139.

Bouillon, S., Connolly, R., Lee, S., 2008. Organic matter exchange and cycling in mangrove ecosystems: recent insights from stable isotope studies. J. Sea Res. 59, 44–58.

Bouillon, S., Connolly, R., Gillikin, D., 2011. 7.07 Use of stable isotopes to understand food webs and ecosystem functioning in estuaries. Treatise Estuar. Coast Sci. 7.

Castañeda-Moya, E., Twilley, R.R., Rivera-Monroy, V.H., Zhang, K., Davis, S.E., Ross, M., 2010. Sediment and nutrient deposition associated with hurricane wilma in mangroves of the Florida coastal Everglades. Estuar. Coast 33, 45–58.

Castañeda-Moya, E., Twilley, R.R., Rivera-Monroy, V.H., 2013. Allocation of biomass and net primary productivity of mangrove forests along environmental gradients in the Florida Coastal Everglades, USA. For. Ecol. Manag. 307, 226–241.

Castañeda-Moya, E., Rivera-Monroy, V.H., Chambers, R.M., Zhao, X., Lamb-Wotton, L., Gorsky, A., Gaiser, E.E., Troxler, T.G., Kominoski, J.S., Hiatt, M., 2020. Hurricanes fertilize mangrove forests in the Gulf of Mexico (Florida Everglades, USA). Proceedings of the National Academy of Sciences.

Childers, D.L., 2006. A synthesis of long-term research by the Florida Coastal Everglades LTER Program. Hydrobiologia 569, 531–544.

Cloern, J.E., Canuel, E.A., Harris, D., 2002. Stable carbon and nitrogen isotope composition of aquatic and terrestrial plants of the San Francisco Bay estuarine system. Limnol. Oceanogr. 47, 713–729.

Coplen, T.B., Kendall, C., Hopple, J., 1983. Comparison of stable isotope reference samples. Nature 302, 236.

Danielson, T.M., Rivera-Monroy, V.H., Castañeda-Moya, E., Briceño, H., Travieso, R., Marx, B.D., Gaiser, E., Farfán, L.M., 2017. Assessment of Everglades mangrove forest resilience: implications for above-ground net primary productivity and carbon dynamics. For. Ecol. Manag. 404, 115–125.

Dawson, T.E., Siegwolf, R., 2011. Stable Isotopes as Indicators of Ecological Change. Academic Press.

Diefendorf, A.F., Freimuth, E.J., 2017. Extracting the most from terrestrial plant-derived n-alkyl lipids and their carbon isotopes from the sedimentary record: a review. Org. Geochem. 103, 1–21.

Diefendorf, A.F., Mueller, K.E., Wing, S.L., Koch, P.L., Freeman, K.H., 2010. Global patterns in leaf 13C discrimination and implications for studies of past and future climate. Proc. Natl. Acad. Sci. Unit. States Am. 107, 5738–5743.

Diefendorf, A.F., Freeman, K.H., Wing, S.L., Graham, H.V., 2011. Production of n-alkyl lipids in living plants and implications for the geologic past. Geochem. Cosmochim. Acta 75, 7472–7485.

Eglinton, T.I., Eglinton, G., 2008. Molecular proxies for paleoclimatology. Earth Planet Sci. Lett. 275, 1–16.

Ficken, K.J., Li, B., Swain, D., Eglinton, G., 2000. An n-alkane proxy for the sedimentary input of submerged/floating freshwater aquatic macrophytes. Org. Geochem. 31, 745–749.

Fry, B., Bern, A., Ross, M., Meeder, J., 2000. δ15N studies of nitrogen use by the red mangrove, Rhizophora mangle L. in south Florida. Estuarine. Coastal Shelf Sci. 50, 291–296.

Gao, L., Huang, Y., 2013. Inverse gradients in leaf wax δD and δ 13 C values along grass blades of Miscanthus sinensis: implications for leaf wax reproduction and plant physiology. Oecologia 172, 347–357.

He, D., Mead, R.N., Belicka, L., Pisani, O., Jaffé, R., 2014. Assessing source contributions to particulate organic matter in a subtropical estuary: a biomarker approach. Org. Geochem. 75, 129–139.

He, D., Simoneit, B.R., Jara, B., Jaffé, R., 2015a. Compositions and isotopic differences of iso-and anteiso-alkanes in black mangroves (Avicennia germinans) across a salinity gradient in a subtropical estuary. Environ. Chem. 13, 623–630.

He, D., Simoneit, B.R., Jara, B., Jaffé, R., 2015b. Occurrence and distribution of monomethylalkanes in the freshwater wetland ecosystem of the Florida Everglades. Chemosphere 119, 258–266.

He, D., Anderson, W.T., Jaffé, R., 2016. Compound specific δD and δ 13 C analyses as a tool for the assessment of hydrological change in a subtropical wetland. Aquat. Sci. 78, 809–822.

He, D., Ladd, S.N., Sachs, J.P., Jaffé, R., 2017. Inverse relationship between salinity and 2H/1H fractionation in leaf wax n-alkanes from Florida mangroves. Org. Geochem. 110, 1–12.

He, D., Zhang, K., Tang, J., Cui, X., Sun, Y., 2018. Using fecal sterols to assess dynamics of sewage input in sediments along a human-impacted river-estuary system in eastern China. Sci. Total Environ. 636, 787–797.

Kahmen, A., Schefuß, E., Sachse, D., 2013. Leaf water deuterium enrichment shapes leaf wax n-alkane δD values of angiosperm plants I: experimental evidence and mechanistic insights. Geochem. Cosmochim. Acta 111, 39–49.

Ladd, S.N., Sachs, J.P., 2013. Positive correlation between salinity and n-alkane δ13C values in the mangrove Avicennia marina. Org. Geochem. 64, 1–8.

Lin, G., Sternberg, L.D.L, 1992a. Differences in morphology, carbon isotope ratios, and photosynthesis between scrub and fringe mangroves in Florida, USA. Aquat. Bot. 42, 303–313.

Lin, G., Sternberg, L.D.L, 1992b. Effect of growth form, salinity, nutrient and sulfide on photosynthesis, carbon isotope discrimination and growth of red mangrove (Rhizophora mangle L.). Funct. Plant Biol. 19, 509–517.

Lovelock, C.E., Ball, M.C., Feller, I.C., Engelbrecht, B.M., Ling Ewe, M., 2006. Variation in hydraulic conductivity of mangroves: influence of species, salinity, and nitrogen and phosphorus availability. Physiol. Plantarum 127, 457–464.

Mancera-Pineda, J.E., Twilley, R.R., Rivera-Monroy, V.H., 2009. Carbon (δ13C) and Nitrogen (δ15N) isotopic discrimination in mangroves in Florida coastal Everglades as a function of environmental stress. Contrib. Mar. Sci. 38, 109–129.

McCarroll, D., Loader, N.J., 2004. Stable isotopes in tree rings. Quat. Sci. Rev. 23, 771–801.

McKee, K.L., Feller, I.C., Popp, M., Wanek, W., 2002. Mangrove isotopic (δ15N and δ13C) fractionation across a nitrogen vs. phosphorus limitation gradient. Ecology 83, 1065–1075.

Mead, R., Xu, Y., Chong, J., Jaffé, R., 2005. Sediment and soil organic matter source assessment as revealed by the molecular distribution and carbon isotopic composition of n-alkanes. Org. Geochem. 36, 363–370.

Medina, E., Fernandez, W., Barboza, F., 2015. Element uptake, accumulation, and resorption in leaves of mangrove species with different mechanisms of salt regulation. Web Ecol. 15 (1), 3–13, 15, 3-13.

Meyers, P.A., 2003. Applications of organic geochemistry to paleolimnological reconstructions: a summary of examples from the Laurentian Great Lakes. Org. Geochem. 34, 261–289.

Rao, Z., Zhu, Z., Wang, S., Jia, G., Qiang, M., Wu, Y., 2009. CPI values of terrestrial higher plant-derived long-chain n-alkanes: a potential paleoclimatic proxy. Front. Earth Sci. China 3, 266–272.

Rivera-Monroy, V.H., Twilley, R.R., Davis III, S.E., Childers, D.L., Simard, M., Chambers, R., Jaffe, R., Boyer, J.N., Rudnick, D.T., Zhang, K., 2011. The role of the Everglades Mangrove Ecotone Region (EMER) in regulating nutrient cycling and wetland productivity in south Florida. Crit. Rev. Environ. Sci. Technol. 41, 633–669.

Rivera-Monroy, V.H., Castañeda-Moya, E., Barr, J.G., Engel, V., Fuentes, J.D., Troxler, T. G., Twilley, R.R., Bouillon, S., Smith, T.J., O'Halloran, T.L., 2013. Current methods to evaluate net primary production and carbon budgets in mangrove forests. Methods Biogeochem. Wetl. 243–288.

Rivera-Monroy, V.H., Lee, S.Y., Kristensen, E., Twilley, R.R., 2017. Mangrove Ecosystems: a Global Biogeographic Perspective. Springer.

Rivera-Monroy, V.H., Danielson, T.M., Castañeda-Moya, E., Marx, B.D., Travieso, R., Zhao, X., Gaiser, E.E., Farfan, L.M., 2019. Long-term demography and stem productivity of Everglades mangrove forests (Florida, USA): resistance to hurricane disturbance. For. Ecol. Manag. 440, 79–91.

Roth, L.C., 1992. Hurricanes and mangrove regeneration: effects of Hurricane Joan, October 1988, on the vegetation of Isla del Venado, Bluefields, Nicaragua, pp. 375–384. Biotropica.

Rovai, A., Riul, P., Twilley, R., Castañeda-Moya, E., Rivera-Monroy, V., Williams, A., Simard, M., Cifuentes-Jara, M., Lewis, R., Crooks, S., 2016. Scaling mangrove aboveground biomass from site-level to continental-scale. Global Ecol. Biogeogr. 25, 286–298.

Rudnick, D.T., Chen, Z., Childers, D., Fontaine, T., 1999. Phosphorus and nitrogen inputs to Florida Bay: the importance of the Everglades watershed. Estuaries 22, 398–416.

Schmitz, N., Verheyden, A., Beeckman, H., Kairo, J.G., Koedam, N., 2006. Influence of a salinity gradient on the vessel characters of the mangrove species Rhizophora mucronata. Ann. Bot. 98, 1321–1330.

Simard, M., Zhang, K., Rivera-Monroy, V.H., Ross, M.S., Ruiz, P.L., Castañeda-Moya, E., Twilley, R.R., Rodriguez, E., 2006. Mapping height and biomass of mangrove forests in Everglades National Park with SRTM elevation data. Photogramm. Eng. Rem. Sens. 72, 299–311.

Simard, M., Fatoyinbo, L., Smetanka, C., Rivera-Monroy, V.H., Castañeda-Moya, E., Thomas, N., Van der Stocken, T., 2019. Mangrove canopy height globally related to precipitation, temperature and cyclone frequency. Nat. Geosci. 12, 40.

Smith, T.J., Anderson, G.H., Balentine, K., Tiling, G., Ward, G.A., Whelan, K.R., 2009. Cumulative impacts of hurricanes on Florida mangrove ecosystems: sediment deposition, storm surges and vegetation. Wetlands 29, 24.

Sobrado, M., 1999. Drought effects on photosynthesis of the mangrove, Avicennia germinans, under contrasting salinities. Trees (Berl.) 13, 125–130.

Sterner, R.W., Elser, J.J., 2002. Ecological Stoichiometry: the Biology of Elements from Molecules to the Biosphere. Princeton university press.

Sun, Z., Livingston, N., Guy, R., Ethier, G., 1996. Stable carbon isotopes as indicators of increased water use efficiency and productivity in white spruce (Picea glauca (Moench) Voss) seedlings. Plant Cell Environ. 19, 887–894.

Troxler, T.G., Gaiser, E., Barr, J., Fuentes, J.D., Jaffe, R., Childers, D.L., Collado-Vides, L., Rivera-Monroy, V.H., Castaneda-Moya, E., Anderson, W., 2013. Integrated carbon budget models for the Everglades terrestrial-coastal-oceanic gradient: current status and needs for inter-site comparisons. Oceanography 26, 98–107.

Twilley, R.R., Rivera-Monroy, V.H., 2009. Ecogeomorphic models of nutrient biogeochemistry for mangrove wetlands. In: Coastal Wetlands: an Integrated Ecosystem Approach. Elsevier, Amsterdam, p. 641.

Twilley, R.R., Rivera-Monroy, V.H., Rovai, A.S., Castañeda-Moya, E., Davis, S., 2019. Mangrove Biogeochemistry at Local to Global Scales Using Ecogeomorphic Approaches, Coastal Wetlands. Elsevier, pp. 717–785.

Wanless, H.R., Parkinson, R.W., Tedesco, L.P., 1994. Sea level control on stability of Everglades wetlands. In: Everglades: the Ecosystem and its Restoration. St. Lucie Press, Delray Beach, FL, USA, pp. 199–223.

Webb, E.L., Friess, D.A., Krauss, K.W., Cahoon, D.R., Guntenspergen, G.R., Phelps, J., 2013. A global standard for monitoring coastal wetland vulnerability to accelerated sea-level rise. Nat. Clim. Change 3, 458–465.

Werner, C., Schnyder, H., 2012. Progress and challenges in using stable isotopes to trace plant carbon and water relations across scales. Biogeosciences 9, 3083–3111.

Yao, Q., Liu, K.-b., Platt, W.J., Rivera-Monroy, V.H., 2015. Palynological reconstruction of environmental changes in coastal wetlands of the Florida Everglades since the mid-Holocene. Quat. Res. 83, 449–458.